

## PATCH ANTENNA ON SPHERE OF BROAD BEAMWIDTH

Hiroyuki Arai and Naohisa Goto  
 Department of Electrical and Electronic Engineering,  
 Tokyo Institute of Technology  
 Ohokayama, Meguro-ku, Tokyo 152, Japan

## 1. INTRODUCTION

The mobile antennas of global positioning system (GPS) should have broad beamwidth to catch the signal from the satellite. Some wire antennas have broad beamwidth, however, flat or conformal antennas are favorable structure for the future application. The radiation beamwidth of the patch antenna, one of the popular flat antennas, is not expanded by the edge diffraction of the grand plane. To obtain the broad beamwidth for the patch antenna, this paper proposes a patch antenna on a perfectly conducting sphere free from the edge diffraction.

## 2. RESONANT MODE

Figure 1 shows the patch antenna on the perfectly conducting sphere. Here, the patch conforms to the thin dielectric on the sphere. The cross section of the antenna is shown in Fig. 2. When the distance  $h$  between the patch and the sphere is much smaller than the sphere radius, a thin cavity with magnetic wall at  $\theta=\alpha$  may be assumed in region  $a \leq r \leq a+h$ ,  $0 \leq \theta \leq \alpha$ , and  $0 \leq \phi \leq 2\pi$ . The resonant modes in the cavity are TM modes ( $H_r=0$ ), and are obtained by solving the following equation.

$$\frac{d}{d\theta} P_v^m(\cos\theta) = 0, \quad (ka)^2 = v(v+1) \quad (1)$$

where  $P_v^m(\cos\theta)$  is the associated Legendre function, and  $k=\omega\sqrt{\epsilon\mu}$ .

The transcendental equation of  $TM_{1n}$  modes for  $v$  is given by (2).

$$\{(v+1)x^2 - v\}P_v(x) - xP_{v+1}(x) = 0, \quad x = \cos(\theta) \quad (2)$$

The solid line in Fig. 3 shows the first root of (2) ( $n=1$ ), the dominant resonant mode, the dependence of patch angle  $\alpha$ , where the root  $v$  is converted into  $ka$  by using (1). The value of  $ka$  is rapidly decreased for  $0 < \alpha < 90$ , while it is almost constant for  $\alpha > 90$ . The dotted line shows  $kl$ , and  $l$  is the length along the patch surface shown in Fig. 2. The value of  $kl$  for small  $\alpha$  is close to 1.841, the resonant mode of circular microstrip disk. As the limiting case  $ka \rightarrow \infty$ , the analysis model is identical with the circular patch on the infinite grand plane.

The quality factor  $Q$  and radiation efficiency  $\eta$  of the cavity filled with dielectric  $\epsilon_r=2.6$  is shown in Fig. 4 for three kinds of cavity height. The radiation power of the antenna is calculated by using the radiation field presented in the next section, and the fields in the cavity are calculated by the planar circuit technique. The  $Q$  is increased, and  $\eta$  is decreased for  $\alpha > 50$ , since the dielectric loss in the

cavity becomes the main factor of  $Q$  and  $\eta$  for large  $\alpha$ . Figure 4 shows that the patch antenna on sphere has  $Q$  and  $\eta$  almost the same with the microstrip patch antenna.

### 3. RADIATION PATTERN

Radiation pattern of the patch antenna on sphere is calculated by assuming a magnetic current loop at  $\theta=\alpha$ ,  $0\leq\phi\leq 2\pi$  on the sphere. This magnetic current loop is identical with that of a slot on the sphere presented by Mushiake and Webster [1]. The radiation patterns of dominant mode of the patch on sphere are obtained by equations (11) and (12) in reference [1] for  $m=1$ .

Figure 5 shows the E and H plane patterns of the patch antenna on the sphere for the patch angle  $\alpha=20, 40,$  and  $60$ , where the relative dielectric constant in the cavity is 2.6. The radiation pattern in E and H plane of the small patch angle is close to that of magnetic current loop of radius  $\cos(\alpha)a/\sqrt{\epsilon_r}$  in free space, however, null angle of the pattern is appeared at  $\theta>90$  for both plane patterns. The beamwidth is changed by the patch angle  $\alpha$ , and the patterns of  $\alpha=40$  has the maximum beamwidth in Fig. 5. The patterns more than  $-10\text{dB}$  in both planes are broader than those of the microstrip antennas on the small grand plane [2]. On the other hand, the radiation to  $\theta=180$  is increased for the large patch angle. This radiation is assumed to be caused by surface current on the sphere. One technique to suppress the surface current is to use the semisphere instead of the sphere for the patch.

The calculated circular polarization pattern and its axial ratio are shown in Figs. 6 and 7, where the isotropic gain is presented for the circular polarization pattern. The gain of patch angle  $\alpha=40$  is more than  $-3\text{dBi}$ , and its axial ratio is more than  $-3\text{dB}$  for  $\theta<90$ . The axial ratio of  $0\text{dB}$  is obtained for  $\theta<60$ , which is a broad beamwidth for the circular polarization. This circular polarization pattern is suitable for mobile antenna for the GPS system.

### 4. CONCLUSION

This paper has presented the patch antenna on the sphere to obtain the broad beamwidth pattern free from the edge diffraction of the grand plane of patch antennas. Resonant modes of the antenna is calculated by the cavity model with magnetic wall, and the radiation pattern by the slot on sphere. Numerical results show that the antenna of small patch angle has broad beamwidth, which is useful pattern for mobile telecommunication systems.

### REFERENCES

- [1] Y.Mushiake and R.E.Webster, "Radiation characteristics with power gain for slots on a sphere," IRE, Trans. on AP., vol. AP-6, pp.47-55, Jan. 1957.
- [2] M.Haneishi, A.Matui, and S.Saito, "A consideration on miniaturization of microstrip antenna," Trans. IEICE, vol. J71-B, no. 11, pp. 1378-1380, Nov. 1988.

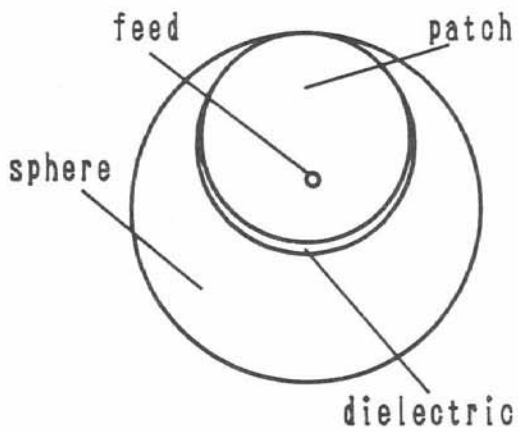


Fig. 1 Patch antenna on sphere.

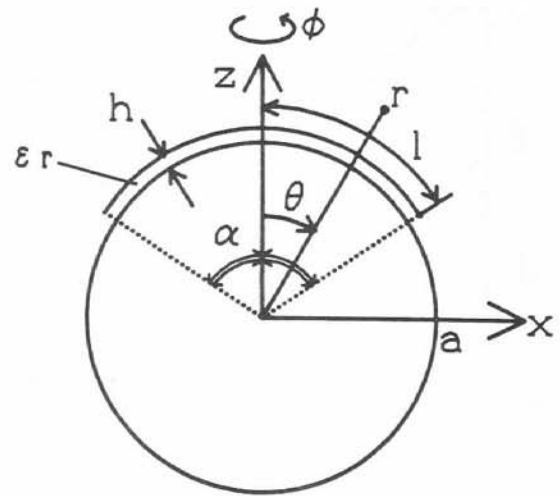


Fig. 2 Cross section of antenna.

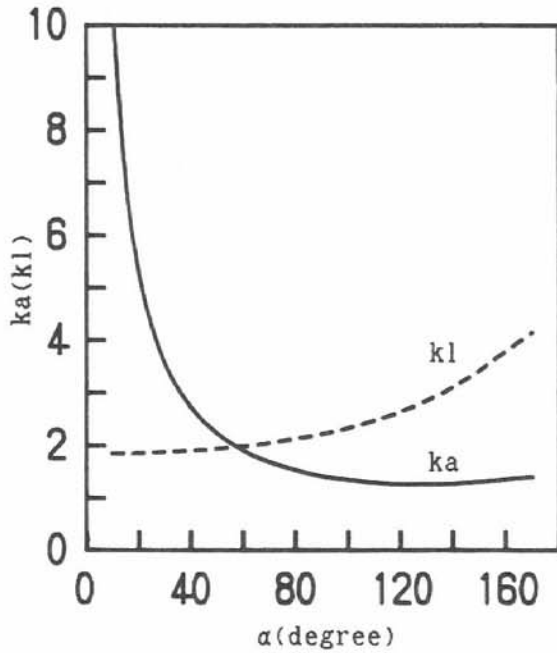


Fig. 3 Resonant  $TM_{11}$  mode versus  $\alpha$ .

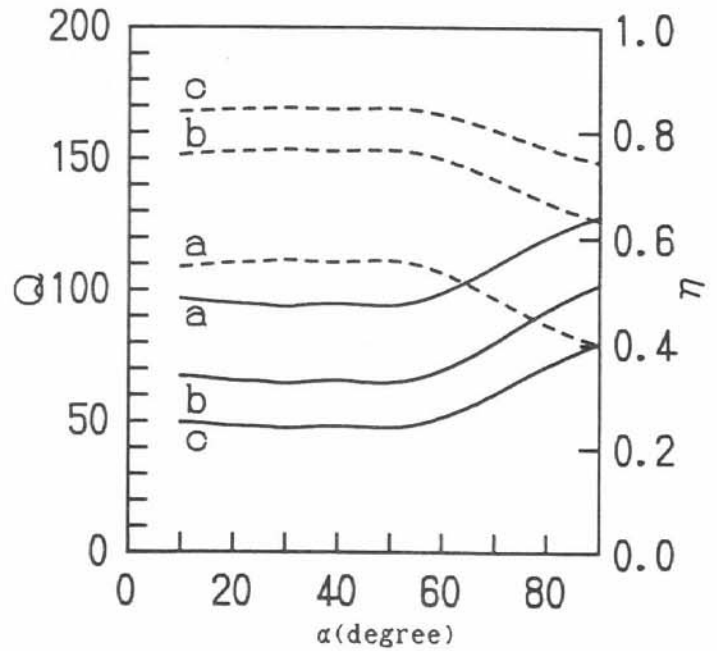
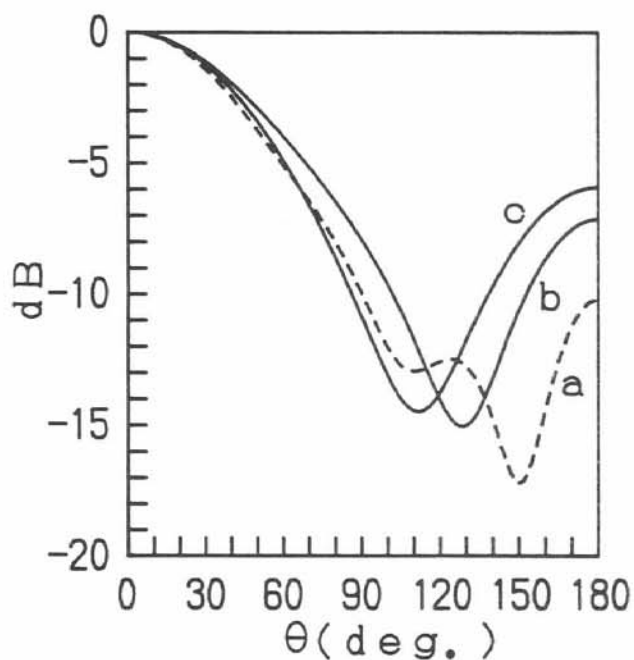
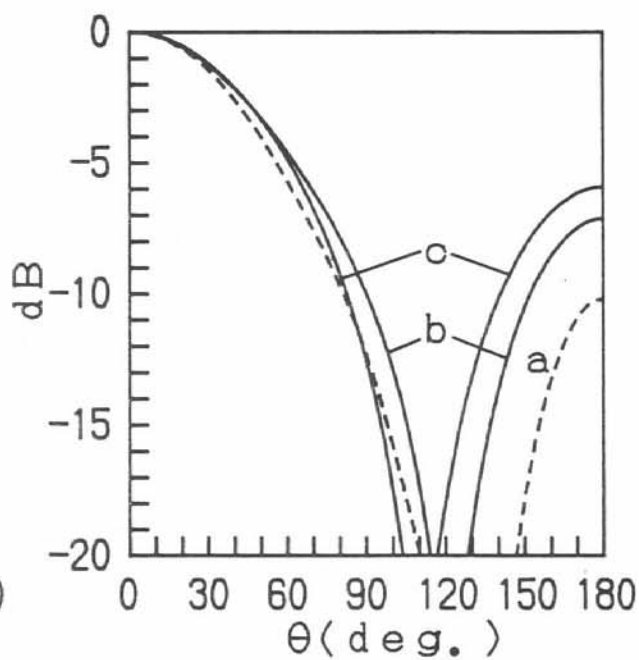


Fig. 4 Quality factor (—) and radiation efficiency (---) versus  $\alpha$ ,  $\epsilon_r=2.6$ ,  $f=1.5\text{GHz}$ ,  $\tan\delta=0.0025$ ,  $a: h=0.01\lambda$ ,  $b: h=0.02\lambda$ ,  $c: h=0.03\lambda$ .



(a) E plane pattern.



(b) H plane pattern.

Fig. 5 Radiation pattern,  
a:  $\alpha=20$ , b:  $\alpha=40$ , c:  $\alpha=60$ .

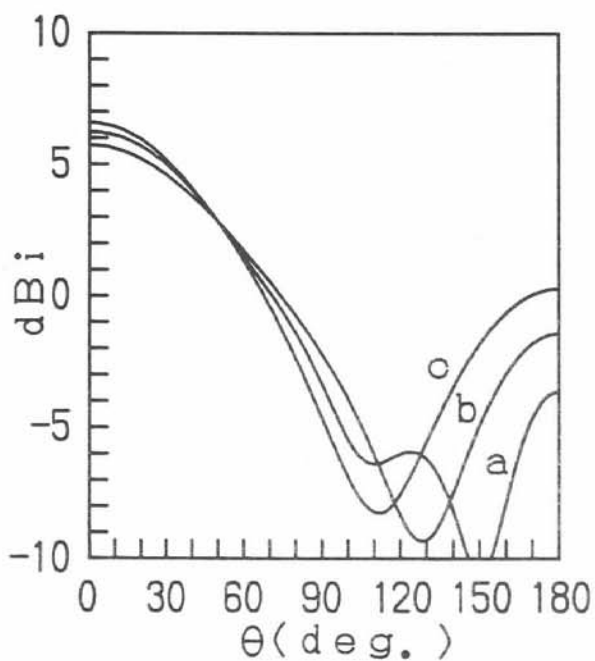


Fig. 6 Circular polarization pattern.  
a:  $\alpha=20$ , b:  $\alpha=40$ , c:  $\alpha=60$ .

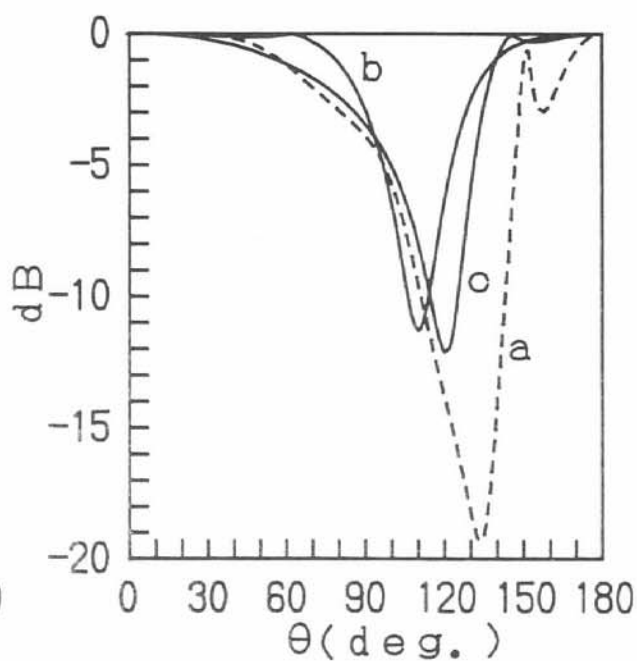


Fig. 7 Axial ratio.  
a:  $\alpha=20$ , b:  $\alpha=40$ , c:  $\alpha=60$ .